Manuscript type: Research Advances

Title:

Identification of organ-specific transcriptomic shifts in the vasculature during systemic inflammation using TrendCatcher

Authors:
Xinge Wang[1], Mark Sanborn[1, 2, 3], Yang Dai[1] and Jalees Rehman[1, 2, 3*]
Xinge Wang: xwang234@uic.edu, Mark Sanborn (msanbo2@uic.edu), Yang Dai: (yangdai@uic.edu), Jalees Rehman: jalees@uic.edu
[1] Department of Bioengineering, The University of Illinois College of Engineering and College of Medicine, Chicago, IL, USA

[2] Department of Pharmacology and Regenerative Medicine, University of Illinois College of Medicine, Chicago, IL, USA

[3] Division of Cardiology, Department of Medicine, University of Illinois College of Medicine, Chicago, IL, USA

*Please address correspondence to: Jalees Rehman (jalees@uic.edu)

The University of Illinois at Chicago, College of Medicine (M/C 868)
835 S. Wolcott Ave. Rm. E403, Chicago, IL 60612, USA
Office phone: +1 312-996-5552; Fax: +1 312-996-1225

Keywords:
Endothelial cells
Endothelial heterogeneity
RNA-seq
Differential expression
Dynamic programming
Vascular biology
Inflammation
Transcription
Translation
Systems biology
Pathway analysis
Brain endothelium
Heart endothelium
Lung endothelium

Abstract

A recent analysis of endothelial cell (EC) gene expression suggests that ECs of distinct organs vary in their gene expression profiles and respond distinctly to the systemic inflammatory stimulus of endotoxemia (Jambusaria et al., 2020). There is a need to systematically define tissue-specific gene expression dynamics in response to inflammation but such an analysis is in part limited by the availability of appropriate algorithms to analyze differential expression across a time course. Here, we present *TrendCatcher* (https://jaleesr.github.io/TrendCatcher_1.0.0/), an R package designed for time course RNA-seq data analysis which identifies distinct dynamic transcriptional programs. When applied to ECs, we observed that approximately 85-95% of EC genes in all three organs followed a biphasic response following endotoxemia. The rapid upregulation of innate immune response and bacterial response genes occurred within 6 hours in all three vascular beds but the subsequent upregulation of reparative EC mitosis and cell cycle genes occurred most rapidly in lung ECs (24-48h) and was most delayed in cardiac ECs (72h-168h). The distinct kinetics of EC inflammatory injury and regeneration identify vascular-bed specific temporal windows for targeted therapeutics.

59 **Introduction**

60 Endothelial cells (ECs) form the inner cellular lining of all blood vessels and establish a barrier
61 between the circulating blood and the underlying parenchyma (Aird, 2012; Bautch, 2011). ECs
62 perform a wide range of critical functions in many physiological processes, such as maintaining
63 intravascular homeostasis, trafficking nutrients and waste between blood and the parenchymal
64 tissues, as well as initiating and regulating immune responses (Liao, 2013). Despite sharing
65 numerous essential roles in physiology, ECs exhibit distinct molecular and functional properties
66 across different tissue types and vascular locations (Nolan et al., 2013; Potente & Mäkinen, 2017).
67 EC heterogeneity has been validated and characterized in both within-organ and organ-specific
68 scenarios. For example, studies focused on characterizing EC heterogeneity within single organs
69 (Sabbagh et al., 2018; Su et al., 2018; Vanlandewijck et al., 2018) have revealed that local cues
70 from the tissue microenvironment, such as metabolites, cell-cell interactions, and cell-matrix
71 interactions, are critical for EC heterogeneity (Lukowski et al., 2019; Potente & Mäkinen, 2017; N.
72 Yucel et al., 2020). The heterogeneity of the microvascular endothelium across organs is apparent
73 in the distinct gene expression profiles of ECs from each major organ (Jambusaria et al., 2020;
74 Kalucka et al., 2020; Nolan et al., 2013; Paik et al., 2020).

75 To investigate the transcriptomic basis of EC heterogeneity, unbiased transcriptomic
76 profiling is essential for providing precise insights into the underpinning molecular mechanisms.
77 Bulk RNA sequencing (RNA-seq) and single-cell RNA sequencing (scRNA-seq) provide viable
78 approaches to study global gene expression. Studies using scRNA-seq have characterized
79 transcriptomic signatures of distinct EC subpopulations and the imprinted transcriptome (Kalucka
80 et al., 2020; Paik et al., 2020). However, the isolation of defined cell populations from their
81 physiological tissue context is required to prepare single-cell suspensions (Eberwine, Sul, Bartfai,
82 & Kim, 2014). Disaggregation of ECs for single-cell analysis or for flow cytometry cell sorting
83 results in the loss of homeostatic outside-in signaling cues from neighboring cells and the
84 extracellular matrix, and could thus alter gene expression profiles (Haimon et al., 2018; van den

85 Brink et al., 2017). The complementary approach of RiboTag-based translatome profiling avoids
86 cell removal from their native niche and enables the direct isolation of tissue-specific ribosome-
87 attached mRNAs without cell dissociation (Cleuren et al., 2019; Sanz et al., 2009). More
88 importantly, this genetic approach allows the direct probing of EC heterogeneity *in situ*, so it offers
89 the recovery and sequence analysis to evaluate the program directly from intact organs (Cleuren
90 et al., 2019). A recent study of the translatome in the cardiac endothelium demonstrated that the
91 tissue-specific endothelial gene expression profile is a reflection of signature open chromatin
92 regions within the cardiac endothelium, which are lost once the cardiac endothelium is removed
93 from its native environment and cultured (N. Yucel et al., 2020). Furthermore, RiboTag
94 complements conventional global bulk RNA-seq and scRNA-seq EC transcriptomic analysis by
95 focusing on mRNAs undergoing translation whereas global RNA-Seq analysis and single-cell
96 RNA-Seq analysis provide profiles reflecting total mRNA in a cell (Jambusaria et al., 2020).

97 Recent studies on organ-specific EC transcriptomic profiles have focused on differences
98 between ECs at baseline but there is a growing interest in how organ-specific EC heterogeneity
99 changes in response to a stressor such as inflammation. Which biological responses show similar
100 changes in magnitude and kinetics across endothelial cells from distinct organs and which stress
101 responses demonstrate organ-specific patterns? This has been addressed in part in recent
102 studies (Ajami et al., 2017; Chong, Yu, Brighton, Bear, & Bautch, 2017; Gunawardana et al., 2021;
103 Tombor et al., 2021), but there is a need for a systematic and unbiased analysis of the temporal
104 kinetics of endothelial gene expression across multiple organs. The endothelial RiboTag
105 transcriptome data collected at 6 different time points following induction of endotoxemia from the
106 heart, brain and lung (Jambusaria et al., 2020) is ideally suited to perform a systematic temporal
107 analysis. Such temporal dynamic characterization would capture the timing of cellular stress
108 response programs and provide insights into the heterogeneous organ-specific kinetics of
109 endothelial injury and repair.

110 Analysis of time-course RNA-seq data represents a computational challenge. Currently,
111 there are mainly two strategies to address these challenges. One strategy treats sampling time
112 points as categorical variables and is based on generalized linear models (GLMs). For example,
113 the software packages DESeq2(Love, Huber, & Anders, 2014), edgeR (McCarthy, Chen, &
114 Smyth, 2012), and limma (Ritchie et al., 2015) use this strategy. These methods focus on the
115 magnitude of change instead of the time order of gene expression, and may also suffer from a
116 relative loss of statistical testing power, especially if many time points are assessed (Fischer,
117 Theis, & Yosef, 2018). A complementary strategy is to treat time as a continuous variable and fit
118 the time expression data into a spline-like model. Such methods include DESeq2Spline (DESeq2
119 adopted with spline model for temporal RNA-seq datasets) fitting, ImpulseDE2 (Fischer et al.,
120 2018) and Next maSigPro (Nueda, Tarazona, & Conesa, 2014). We found the latter strategy
121 increased the power of detecting dynamic genes, but it may suffer from a strong model
122 assumption that oversimplifies the complicated dynamic biological scenarios, such as multiphasic
123 responses in which gene expression patterns can oscillate between rapid increases and
124 decreases to reflect initial responses as well as counter-regulatory compensatory responses.
125 In our present study, we developed TrendCatcher, a versatile R package tailored for time-
126 course RNA-seq analysis. TrendCatcher uses a framework that combines the smooth spline
127 ANOVA model and break point searching strategy which identifies inflection points when gene
128 expression trends reverse. We show that TrendCatcher outperformed the leading methods for
129 time-course RNA-Seq analysis by using simulated time course data. TrendCatcher has the unique
130 ability to show users changes in biological pathway enrichment over time, which highlights the
131 distinct transcriptional programs that are associated with dynamic biological processes. We
132 applied TrendCatcher to the gene expression profiles of ECs from the brain, heart, and lung EC
133 and identified the kinetics of injury, repair, and regeneration programs.
134
135

136 **Results**

137 **TrendCatcher accurately identifies dynamic differentially expressed genes (DDEGs) in**
138 **simulated datasets**

139 First, we tested the prediction performance of the TrendCatcher platform (**Figure 1**) using a set
140 of simulated time course RNA-seq datasets, because simulated data provides defined standards
141 to assess the accuracy of novel analytical platforms. We considered a comprehensive collection
142 of gene temporal trajectory patterns to simulate a set of realistic data with biological
143 characteristics (Bar-Joseph, Gitter, & Simon, 2012). We embedded 1,000 constant trajectories
144 (non-dynamic genes), 500 linear trajectories (monotonous state transition, i.e. continuously
145 increasing or continuously decreasing gene expression levels throughout the time course), 500
146 impulse shaped single break point trajectories (only one temporal inflection point, i.e. up-peak-
147 down or down-trough-up), 500 two break point trajectories and 500 three break point trajectories
148 (more complicated dynamic response, e.g., a combination of 2 or more basic types of trajectories).
149 As shown in **Figure 2A-C**, compared to DESeq2, DESeq2Spline and ImpulseDE2, TrendCatcher
150 achieved higher accuracy in a mixed simulated dataset. We also tested each model's
151 performance on a varying number of time points. As shown in **Figure 2D**, TrendCatcher had the
152 highest prediction accuracy across all time points tested, with accuracies of more than 75%.

153 We also generated 1,000 gene trajectories for each type of dynamic profile to compare
154 each model's performance across different trajectory types. As shown in **Figure 2—figure**
155 **supplement 1A-B**, for basic trajectory patterns, such as linear trajectory and impulse shaped
156 trajectory, TrendCatcher achieved accuracies of 80.8% for linear trajectory and 75.3% for impulse
157 shaped trajectories. As shown in **Figure 2—figure supplement 1C-D**, 2 to 3 break points
158 represent the combination of basic temporal trends, such as an impulse response leading to
159 another sustained response. TrendCatcher had higher prediction accuracies of 94.2% for two
160 break points trajectories and 91.4% for three break points trajectories and thus outperformed the
161 other three models. Interestingly, DESeq2 and DESeq2Spline works well only when the trajectory

162 pattern is simple, but we observed their accuracies dropped for more general trajectory types. For
163 example, DESeq2Spline prediction accuracy dropped to 62.46% in the three break point dynamic
164 pattern. These results suggest that TrendCatcher can maintain its accuracy even in the setting of
165 various complex temporal patterns (with multiple break or inflection points), which may occur in
166 the setting of early biological responses followed by counter-regulatory adaptive responses.
167
168 **TrendCatcher identifies in situ organ-specific DDEGS and their temporal patterns**
169 **composition during inflammatory injury**
170 We applied TrendCatcher to the previously reported RiboTag dataset of the endothelial
171 translatome in the murine heart, brain and lungs during baseline and endotoxemia (Jambusaria
172 et al., 2020) to identify dynamic inflammatory response genes. The RiboTag dataset
173 (GSE136848) is an RNA-seq dataset of *in situ* endothelial cell response to systemic injury induced
174 by sublethal intraperitoneal bacterial endotoxin lipopolysaccharide (LPS) at six time points and
175 across three distinct vascular beds during homeostasis and inflammation. We analyzed the global
176 transcriptomics profiles at 0 hour (baseline), 6 hours, 24 hours, 48 hours, 72 hours and 168 hours
177 after LPS-injury to the brain, heart and lung. TrendCatcher identified 2,047 significantly dynamic
178 genes in brain ECs (**Supplementary file 1**), 2,044 dynamic genes in heart ECs (**Supplementary**
179 **file 2**), and 2,632 dynamic genes in lung ECs (**Supplementary file 3**). They accounted for 11.3%,
180 13.4% and 16.2% of the total expression profiles of brain, heart and lung, respectively, suggesting
181 that over 80% of the expressed genes in the endothelium only fluctuate around baseline
182 expression level in response to the profound inflammatory injury.
183 TrendCatcher also assigned trajectory pattern types to all dynamic genes identified from
184 post LPS-injury, and provided hierarchical pie charts to visualize the composition of trajectory
185 patterns across the three organs. Each dynamic gene's trajectory pattern was characterized using
186 a hierarchical scheme, a master-pattern type and a sub-pattern type. A master-pattern type
187 describes the basic type of gene expression trend, for example, "up-down" represents a biphasic

188 response, upregulation followed by downregulation. The sub-pattern type shows the time-
189 dependent dynamic behavior of a gene transcriptional response. For example,
190 "0h_up_24h_down_168h" belongs to an "up-down" master-pattern type and represents peak
191 gene upregulation at 24 hours, followed by downregulation until 168 hours.

192 We observed the same 8 major master-patterns across the three organs (**Figure 3A**) but
193 with sub-pattern composition shifts (**Figure 3—figure supplement 1-3**), especially for "up-down"
194 biphasic response with distinct upregulation time. As the inner hierarchical pie charts of **Figure**
195 **3B-D** show, we found over 85-95% of all the dynamic genes from brain, heart and lung ECs had
196 a biphasic response to LPS-inflammation. The majority of the biphasic response genes were
197 upregulated first, suggesting that there is a clear asymmetry in favor of endothelial gene
198 upregulation instead of gene repression during inflammatory injury. We found that heart and lung
199 ECs tended to have more early-upregulated genes at the first 6 hours (**Figure 3C-D)**, as 51.6%
200 of DDEGs in heart EC and 40% of DDEGs in lung ECs reached the expression peak at 6 hours.
201 In contrast, in brain ECs only 20.3% of DDEGs reached peak expression at 6 hours. Brain EC
202 DDEGs tended to gradually increase their expression level, such that 20% and 20.6% reached
203 peak expression 24 hours and 48 hours after induction of inflammatory LPS-injury.

204
205
206 **Organ-universal and organ-specific inflammatory shift using genes from the same**
207 **temporal pattern**

208 We further investigated whether dynamic genes across brain, heart and lung ECs share similar
209 biological functions by exploring organ-universal inflammation pathways. We assessed the
210 overlap among the three EC types for each sub-pattern gene trajectory and performed a gene
211 ontology (GO) enrichment analysis. We found 143 "universal" (i.e. across ECs in all three organs)
212 dynamic genes (**Figure 4A, Supplementary file 4**) in the early 6-hour activation sub-pattern
213 ("0h_up_6h_down_168h") which were enriched for self-defense-related pathways. These
214 included response to lipopolysaccharide (19 genes), defense response to virus (27 genes) and

215 response to interferon-beta (14 genes), response to interferon-gamma (17 genes) (**Figure 4B**).
216 These shared early activation pathways suggest an organ-universal mechanism to LPS-induced
217 inflammatory injury, in which ECs across multiple major organs activate self-defense pathways
218 shortly after injury, with a strong enrichment of interferon response genes.

219 We also assessed organ-specific pathways that were upregulated early on at 6 hours after
220 LPS injury. Brain-specific inflammatory responses were enriched for increased neutrophil
221 migration and regulation of angiogenesis (**Figure 4C**). However, pathways related to Wnt
222 signaling were downregulated (**Figure 4-figure supplement 1B**), which is important because
223 Wnt signaling is a key regulator of the integrity of the blood brain barrier (BBB) (Laksitorini,
224 Yathindranath, Xiong, Hombach-Klonisch, & Miller, 2019). Early-peaking heart-specific EC
225 responses were highly enriched in ribosome assembly and ribosome biogenesis processes
226 suggesting global upregulation of protein translation (**Figure 4D**), but showed an early
227 downregulation in cytokinesis pathways (**Figure 4-figure supplement 1C**). In lung ECs, we
228 observed the unique upregulation of leukocyte, neutrophil, and granulocyte migration and
229 chemotaxis, and pathways related to calcium ion homeostasis (**Figure 4E**), whereas endothelial
230 cell migration gene expression was downregulated (**Figure 4-figure supplement 1D**).

231 At 24h, brain ECs upregulated ribosome biogenesis processes, mirroring the upregulation
232 of these processes that we had observed in heart ECs at the earlier 6h time point (**Figure 4-figure**
233 **supplement 2B)**. At this time point, heart ECs concomitantly upregulated ER stress response
234 pathways as well as proteasomal degradation pathways (**Figure 4-figure supplement 2C**). In
235 lung ECs, the bulk of upregulated genes occurred at the 6h time point but we also identified
236 selected genes peaking later at 24h, however they were also related to pro-inflammatory
237 processes such as leukocyte migration (**Figure 4-figure supplement 2D**), suggesting that
238 compared to the heart and the brain, the lung endothelium showed the most prominent sustained
239 upregulation of pro-inflammatory genes during 6h-24h.

240

241 **Time-Heatmap discloses organ-specific dynamic programming of endothelial cells**

242 Next, we developed a Time-Heatmap function in TrendCatcher to analyze and visualize the time-
243 dependent dynamic programming. Instead of grouping genes solely based on the trajectory sub-
244 pattern types, which uncovers very few enriched biological pathways, TrendCatcher groups genes
245 based on a derivative manner. It treats neighboring time points as a time window and compares
246 each gene's expression level within the time window to its previous break point expression level.
247 In this way, genes sharing the same expression dynamic within a time window were grouped,
248 independent of their whole dynamic trajectory pattern.

249 We first applied this approach to the lung EC dataset which has exhibited the most
250 prominent and sustained upregulation of inflammatory genes. As shown in **Figure 5**,
251 TrendCatcher captured distinct phases of lung EC inflammation: 1) inflammatory activation and
252 injury responses, 2) EC proliferation and regeneration as well as 3) EC migration and
253 angiogenesis. The enrichment of host-defense pathways, such as innate immune response and
254 response to bacterium, were strongly activated within the 0h-6h time window, and then
255 subsequently downregulated. This is followed by an increase in cell cycle related pathways over
256 the 24h-48h time window, such as cell division and regulation of mitotic cell cycle phase transition.
257 The upregulation of EC migration and angiogenesis during the late phase (72h-168h) suggests
258 that after inflammatory injury and proliferation, repair of the lung endothelial barrier likely involves
259 EC migration.

260 We also applied the Time-Heatmap analysis to brain ECs and heart ECs. We observed a
261 similar juxtaposition of early host-defense responses followed by EC proliferation and
262 regeneration (**Figure 5—figure supplement 1 and 2**). However, the regenerative responses in
263 heart ECs showed a significantly delayed activation which was primarily seen at 168h, i.e., 1 week
264 after the injury.

265 For mechanistic analyses, it is also critical to identify individual genes which drive the
266 biological processes which is why we developed a function allowing for a visualization of fold-

267 change (logFC) expression of enriched gene sets from selected target GO terms. As shown in
268 **Figure 6A**, during the 0-6h time window the GO term defense response was enriched in brain,
269 heart and lung ECs, but in each vascular bed different sets of dynamic genes were involved. For
270 brain ECs (**Figure 6A**), the highly dynamic DDEGs were tumor necrosis factor (Tnf), aconitate
271 decarboxylase 1 (Acod1), interleukin 1 receptor (Il1r2), sialic acid binding Ig-like lectin E (Siglece),
272 chemokine ligand 1 (Cxcl1), interleukin 6 (Il6) and matrix metallopeptidase 12 (Mmp12); For heart
273 ECs (**Figure 6B**), the highly DDEGs are interleukin 18 receptor accessory protein (Il18rap), sialic
274 acid binding Ig-like lectin E (Siglece), interleukin 1 receptor (Il1r2), interleukin 6 (Il6), chemokine
275 ligand 5 (Cxcl5) and N-formyl peptide receptor 2 (Fpr2). Whereas, for lung ECs (**Figure 6C**), top
276 dynamic corresponding genes were triggering receptor expressed on myeloid cells 3 (Trem3),
277 arginase 1 (Arg1), interleukin 1 receptor type 2 (Il1r2), interleukin 10 (Il10), alpha 2-HS
278 glycoprotein (Ahsg). These organ-specific dynamic EC response genes may provide novel
279 vascular-bed novel therapeutic targets.
280

281 **Organ-specific baseline differentially expressed genes (DEGs) temporal behavior**
282 **following endotoxemia**

283 We next focused on the top organ-specific highly expressed differentially expressed genes
284 (DEGs) identified during homeostatic conditions (Jambusaria et al., 2020) to see whether these
285 organ-specific EC signature genes remain stable over time in the setting of inflammation or
286 whether they are also dynamic. For each organ, we focused on the study of the top 10 RiboTag
287 signature genes ranked by their log fold change (logFC) value compared to the other two organs
288 (**Figure 7A, Supplementary file 5**). We found the following selected genes which constitute the
289 organ-specific EC signatures during homeostasis are modulated during inflammatory injury. For
290 brain ECs, 7 out of 10 highly expressed brain EC signature genes were disrupted by the
291 inflammatory process (**Figure 7A, Supplementary file 5**), most of which showed rapid

292 downregulation. Only apolipoprotein D followed an “up-down” pattern, which was upregulated in
293 the first 72 hours after inflammation and returned to baseline after 72 hours. For heart ECs (**Figure**
294 **7B, Supplementary file 5**), butyrophilin like 9 (Btnl9) and aquaporin-7(Aqp7) followed a
295 monotonic increase pattern and increased almost 2-fold at 168 hours after inflammatory
296 activation. For lung ECs (**Figure 7C, Supplementary file 5**), only resistin like alpha (Retnla) was
297 upregulated in the first 6 hours and then downregulated to baseline. In contrast to brain ECs, the
298 top 10 signature genes for heart and lung ECs remained stable during the injury phase suggesting
299 that brain ECs exhibit the greatest vulnerability to losing their homeostatic brain EC signature in
300 the face of systemic LPS injury.
301

302

303 **Discussion**

304 ECs serve as a highly dynamic interface under normal physiological conditions and their organ-
305 specific heterogeneity is essential for organ development, homeostasis, and tissue regeneration
306 (Bautch, 2011). The control of tissue vasculature by ECs is vital for disease states ranging from
307 inflammation to cancer (Augustin & Koh, 2017). ECs regulate inflammation by preventing
308 coagulation, controlling blood flow, and trafficking proteins from blood to tissues (Pober & Sessa,
309 2007). RiboTag RNA-seq profiling enables *in situ* assessment of organ-specific endothelial
310 translatomes (Cleuren et al., 2019), and by performing this analysis across time points, we were
311 able to track how each organ's endothelial translatomes changed over time in response to a
312 stressor. Uncovering how organ-specific ECs respond to inflammation in a time-dependent
313 manner may uncover new therapeutic targets and the corresponding temporal windows.

314 Using our computational platform, TrendCatcher, we identified time-dependent endothelial
315 inflammatory response genes in different organs post endotoxemia, which could be broadly
316 grouped into shared universal response genes across all three endothelial beds as well as
317 response genes that were unique to specific endothelial beds. Approximately 85-95% of all organ-
318 specific dynamic genes responded with biphasic trajectories, and most of the genes responding
319 to LPS-injury reached their peak within 48 hours. We also observed significant universal
320 upregulated inflammatory responses across all endothelial beds, which were host-defense-
321 related pathways. The early host-defense-related dynamic inflammatory markers suggest an
322 organ-universal self-defense mechanism, in which ECs from various vascular beds activate pro-
323 inflammatory cytokines and likely facilitate the migration of immune cells to the infected sites.

324 We observed brain-specific EC downregulation of Wnt pathway genes during early
325 inflammation. Emerging evidence shows crosstalk between oligodendrocytes and ECs, which is
326 mediated by signaling through the Wingless and Int-1(WNT)/beta-catenin pathway (Manukjan,

327 Ahmed, Fulton, Blankesteijn, & Foulquier, 2020). Dysregulation of Wnt signaling results in a
328 breakdown of blood brain barrier function (BBB) (Laksitorini et al., 2019; Martowicz et al., 2019),
329 which is why our observation that Wnt pathway genes were predominantly downregulated in brain
330 ECs is especially intriguing. It may indicate that Wnt downregulation mediates LPS-induced
331 compromise of BBB function and constitutes a point of vulnerability for the brain endothelium.
332 Since BBB integrity can be compromised by endotoxemia and is thought to exacerbate
333 neurodegenerative diseases such as Alzheimer's disease (Barton et al., 2019; L. M. Liu, Wan,
334 Xia, Kalionis, & Li, 2014) the identification of Wnt pathway gene downregulation in our unbiased
335 temporal analysis offers important new therapeutic targets for restoring BBB integrity in
336 endotoxemia.

337 One of the key features of bacteremia and endotoxemia is the compromise of cardiac
338 function (Kakihana, Ito, Nakahara, Yamaguchi, & Yasuda, 2016; G. Yucel et al., 2017). On the
339 one hand, the myocardium responds with hyperdynamic function especially in the setting of
340 systemic vasodilation to maintain systemic perfusion (Kalogeris, Baines, Krenz, & Korthuis, 2012),
341 but prolonged endotoxemia or bacteremia can also lead to stress cardiomyopathy (Jafarzadeh,
342 Thomas, Warren, Gill, & Fraser, 2016; Roivainen et al., 2000). As there is growing evidence that
343 cardiac ECs are key regulators of cardiac function and that loss of cardiac contractility is in part
344 due to a compromise of the cardiac endothelium (Potente & Mäkinen, 2017; N. Yucel et al., 2020),
345 the gene expression changes we observed in cardiac ECs may reflect these distinct phases of
346 endotoxemia or bacteremia. The early rise in ribosome biogenesis genes is followed by ER stress
347 pathway upregulation, which suggests that ER stress in the cardiac endothelium may contribute
348 to myocardial dysfunction during prolonged endotoxemia, and later, at 24 hours, heart EC
349 activated genes were enriched in the endoplasmic reticulum (ER).

350 Lung ECs are of special interest during systemic inflammation and endotoxemia because
351 lung vascular injury is a core pathogenic mechanism in the development of acute respiratory

352 distress syndrome (ARDS). Leukocytes have been shown to migrate to the lung microvasculature
353 and interstitium during acute lung injury (ALI) (Claser et al., 2019; Senaldi, Vesin, Chang, Grau,
354 & Piguet, 1994 Grau, & Piguet, 1994) and the upregulation of calcium signaling increases lung
355 endothelial permeability (Tiruppathi, Minshall, Paria, Vogel, & Malik, 2002), which further
356 exacerbates lung injury by leading to unfettered influx of immune cells and fluid into the lung
357 alveolar space. Importantly, TrendCatcher identified upregulation of lung EC cell cycle pathways
358 at 48h-72h, which coincides with what was recently reported for the kinetics of lung EC
359 regeneration after endotoxemic injury (M. L. Liu et al., 2019).

360 In summary, we have developed a novel computational and visualization tool,
361 TrendCatcher, to facilitate the interpretation of time-course RNA-seq data. TrendCatcher can
362 identify dynamic differentially expressed genes (DDEGs), assign dynamic trajectory patterns to
363 DDEGs, reveal dynamic pattern composition across different experiments, and visualize changes
364 in biological pathway enrichment across multiple time-points. Compared to existing computational
365 tools, it achieved higher prediction power in dynamic gene identification from simulated datasets.
366 Since TrendCatcher assesses distinct time points sequentially and thus maintains a temporal
367 hierarchy, it may be better suited for the identification of complex temporal trajectories than
368 current methods. By allowing users to set fold-change thresholds as well as define a priori gene
369 sets of interest, TrendCatcher is versatile and can be used to mine a variety of temporal RNA-seq
370 datasets. By applying it to EC transcriptomics, we identified injury and regeneration kinetics
371 across various vascular-beds which could pave the way for assessing novel therapeutic targets
372 during defined temporal windows.

373 ## Materials and Methods

374 ### TrendCatcher framework

375 The main components of the TrendCatcher framework are shown in **Figure 1**. TrendCatcher
376 requires two main inputs: the raw count table C of a temporal study with a dimension of $m \times n$,
377 where m denotes the number of genes and n denotes the number of samples, and a user-defined
378 baseline time vector T, such as "0 hour". Since samples may have different sequencing depths
379 and batch effect, TrendCatcher integrates with limma (Ritchie et al., 2015) and provides
380 preprocessing steps. Based on a user-specified threshold, relatively low abundant genes are
381 removed from the count table, and reads are normalized and batch effects are removed.
382 TrendCatcher's core algorithm is composed of five main steps: (a) baseline fluctuation confidence
383 interval estimation, (b) model dynamic longitudinal count, (c) time point dynamic p-value
384 calculation, (d) gene-wise dynamic p-value calculation, and (e) break point screening and gene-
385 wise dynamic pattern assignment. Mathematical details will be expanded in the following sections.
386 For the output of TrendCatcher, there are mainly two components: a master table and a set of
387 functions for versatile visualization purposes. The master table contains all the dynamic details of
388 each single gene, including its dynamic p-value, its break point location time, and its dynamic
389 trajectory pattern. In addition to the master table, TrendCatcher produces three main types of
390 visualizations: (a) a figure showing the observed counts and fitted splines of each gene, (b) a
391 hierarchical pie chart that represents trajectory pattern composition, (c) and a Time-Heatmap of
392 dynamic biological pathway enrichment change over time.

393

394 ### Baseline fluctuation confidence interval estimation

395

396 We assumed that the observed number of RNA-seq reads count from the baseline time (e.g., t=0
397 hour) $X_{i,t_{baseline}}$ was generated from a negative binomial distribution (Equation 1):

$$X_{i,t_{baseline}} \sim NB(\mu_{i,t_{baseline}}, \varphi_i) \quad (1)$$

Where gene $i = 1, \dots, n$ and $\mu_{i,t_{baseline}}$ is the mean count of gene i at baseline time, and φ_i is the dispersion factor. First, the dispersion factor φ_i was pre-estimated as a constant hyperparameter for each gene with DESeq2(Love et al., 2014), as shown in Equation 2. Here, σ_i is the variance.

$$\sigma_i(t)^2 = \mu_i(t) + \varphi_i * \mu_i(t)^2 \quad (2)$$

Then, $\mu_{i,t_{baseline}}$ was estimated using maximum likelihood from Equation 3.

$$\widehat{\mu}_{i,t_{baseline}} = argmax\ L_{NB}(u, \varphi) = argmax\ \frac{\Gamma(\varphi + x)}{x!\,\Gamma(\varphi)} (\frac{\mu}{\mu + \varphi})^x (\frac{\varphi}{\varphi + \mu})^\varphi \quad (3)$$

Based on negative binomial distribution and the estimated mean count for baseline time, we constructed the 95% confidence interval $[X_{i,t_{baseline}},0.05, X_{i,t_{baseline}},0.95]$ as the baseline count fluctuation interval (Equation 4(a) and Equation 4(b)).

$$P\left(x_{i,t_{baseline}} \leq X_{i,t_{baseline}},0.05 \mid \mu_{i,t_{baseline}}, \varphi_i\right) = 0.05 \quad (4a)$$

$$P\left(x_{i,t_{baseline}} \geq X_{i,t_{baseline}},0.95 \mid \mu_{i,t_{baseline}}, \varphi_i\right) = 0.95 \quad (4b)$$

Model dynamic longitudinal count estimation

To model the time dependent gene expression value, we applied a smoothing spline ANOVA model (Gu, 2013; Metwally et al., 2018) with a negative binomial family constrain to fits the reads from samples across non-baseline multiple time points. The random variable $X_{i,t(t \neq t_{baseline})}$ is assumed to follow NB distribution in Equation 5, with a positive integer α represents number of failures before the αth success in a sequential of Bernoulli trials, and $p(t) \in (0,1)$ represents the success probability.

$$X_{i,t(t \neq t_{baseline})} \sim NB(\alpha, p(t)) \quad (5)$$

The log likelihood given a time-course observed count $x = \{x_{i,t(t \neq t_{baseline})}\}_{i=1,\dots,n;\ t=1,\dots,T}$ is calculated as Equation 6.

$$L = log\ L(\alpha, p(t) \mid X = x\ )$$

$$= \sum_{t=1}^{T}\sum_{i=1}^{n}[x_{i,t(t\neq t_{baseline})} \log(1 - p(t) + \alpha log p(t) + log\Gamma\big(\alpha + x_{i,t(t\neq t_{baseline})}\big) - \quad (6)$$

$$loglog\Gamma(\alpha)] + C$$

Taking the logit link and model time effect, we define the logit link η

$$\eta = log\ \frac{p(t)}{1 - p(t)} \quad (7)$$

To allow for flexibility in the estimation of η , and find the best trade-off between goodness of fit and the smoothness of the spline curve, soft constraints of the form $J(\eta)$ is added to the minus log-likelihood, with the smoothing parameter $\lambda > 0$.

$$-L + \lambda\ J(\eta) \quad (8)$$

The solution to the optimization of Equation 8 leads to a smoothing fitting to the reads from samples across different non-baseline time points. The estimated mean of $\mu_{i,t(t\neq t_{baseline})}$ can be estimated using Equation 9.

$$\mu_{i,t(t\neq t_{baseline})} = \hat{\alpha}e^{\hat{\eta}(t)} = \frac{\hat{\alpha}\hat{p}(t)}{1 - \hat{p}(t)} \quad (9)$$

Gene's dynamic p-value calculation

To calculate gene's non-baseline dynamic signal significance, each gene's non-baseline estimated mean count $\mu_{i,t(t\neq t_{baseline})}$ was tested against the baseline fluctuation interval. Based on Equation 10(a) and Equation 10(b), for each gene at each single non-baseline time point, a dynamic time p-value was calculated.

$$If\ \mu_{i,t(t\neq t_{baseline})} \geq \mu_{i,t_{baseline}},\ then\ p_{i,t} = \int P(x \geq \mu_{i,t(t\neq t_{baseline})} \mid \mu_{i,t_{baseline}}, \varphi_i) \quad (10a)$$

$$If\ \mu_{i,t(t\neq t_{baseline})} \leq \mu_{i,t_{baseline}},\ then\ p_{i,t} = \int P(x \leq \mu_{i,t(t\neq t_{baseline})} \mid \mu_{i,t_{baseline}}, \varphi_i) \quad (10b)$$

Then, we applied Fisher's combined probability test method to calculate a gene-wise dynamic p-value (Equation 11):

$$\chi^2_{i,2t} \sim -2\sum_{t=0}^{T} ln\,(p_{i,t}) \tag{11}$$

Trajectory pattern assignment

First, we connect all the significant dynamic signal time points, with a p-value threshold less than 0.05. Then we applied a break point searching strategy to capture the gene expression change trend. The definition of break point is defined using Equation 12(a) and Equation 12(b).

$$If\ \mu_{i,t} > \mu_{i,t_{next}}\ \&\ \mu_{i,t} > \mu_{i,t_{previous}}, break\ point\ type\ I. \tag{12a}$$

$$If\ \mu_{i,t} < \mu_{i,t_{next}}\ \&\ \mu_{i,t} < \mu_{i,t_{previous}}, break\ point\ type\ II. \tag{12a}$$

There are two types of break points, type I means gene up-regulated followed by a down regulation and type II means gene expression level down regulated and then followed by an upregulation. By screening along the break point, the master-pattern and sub-pattern were assigned to each gene.

Time-Heatmap enrichment analysis

To build the Time-Heatmap for visualizing the biological pathway enrichment change over time, we designed a window-sliding strategy to capture all the up-regulated or down-regulated genes for each time interval. If we denote time vector as t_j and $j \in 1, \ldots, T$, each time interval is denoted as $[t_{j-1}, t_j]$. We found N_{up} up-regulated genes and N_{down} down-regulated genes within the time window $[t_{j-1}, t_j]$, then a Fisher's exact test was performed to obtain the Gene Ontology (GO) term enrichment with the corresponding time interval.

446 Besides GO enrichment analysis (Yu, Wang, Han, & He, 2012), TrendCatcher also
447 packed Enrichr (Kuleshov et al., 2016) biological pathway databases.

448 **Simulated dataset**

449 We embedded 5 different types of trajectories into the temporal RNA-seq simulated
450 datasets, including constant trajectory, linear trajectory, impulse trajectory, 2 break-point
451 trajectory and 3 break-point trajectory. Each type of trajectory was constructed by adding
452 negative binomial distribution noise to the embedded trajectory count. We mixed 1,000
453 constant trajectories with the other 4 types of dynamic trajectories (500 from each type).
454 Then, we used a dynamic filter to trajectories to further distinguish constant trajectories
455 versus strong dynamic trajectories. We used log2FC range over the time course less than
456 0.5 as a threshold to relabel constant trajectories and strong dynamic trajectories. We
457 sampled 6 to 10 different number of time points with evenly time intervals, and randomly
458 sampled 3 replicates for each time point.

459 **RiboTag dataset preprocessing and batch correction**

460 We downloaded RiboTag RNA-seq dataset from NCBI-GEO website with the access
461 number GSE136848. We applied limma R package for library normalization and batch
462 correction to the Brain EC, Heart EC and Lung EC respectively. For gene symbol
463 annotation, we used ENSEMBL features from biomaRt (Durinck, Spellman, Birney, &
464 Huber, 2009) package.

465

466

467

468 **Acknowledgments**

469 The studies were supported by NIH grants R01-HL152515 (to JR), R01-HL154538 (to JR), P01-

470 HL060678(to JR) and R01-HL126516 (to JR).

References

Aird, W. C. (2012). Endothelial cell heterogeneity. *Cold Spring Harb Perspect Med, 2*(1), a006429. doi:10.1101/cshperspect.a006429

Ajami, N. E., Gupta, S., Maurya, M. R., Nguyen, P., Li, J. Y. S., Shyy, J. Y. J., . . . Subramaniam, S. (2017). Systems biology analysis of longitudinal functional response of endothelial cells to shear stress. *Proceedings of the National Academy of Sciences of the United States of America, 114*(41), 10990-10995. doi:10.1073/pnas.1707517114

Augustin, H. G., & Koh, G. Y. (2017). Organotypic vasculature: From descriptive heterogeneity to functional pathophysiology. *Science, 357*(6353). doi:10.1126/science.aal2379

Bar-Joseph, Z., Gitter, A., & Simon, I. (2012). Studying and modelling dynamic biological processes using time-series gene expression data. *Nat Rev Genet, 13*(8), 552-564. doi:10.1038/nrg3244

Barton, S. M., Janve, V. A., McClure, R., Anderson, A., Matsubara, J. A., Gore, J. C., & Pham, W. (2019). Lipopolysaccharide Induced Opening of the Blood Brain Barrier on Aging 5XFAD Mouse Model. *Journal of Alzheimers Disease, 67*(2), 503-513. doi:10.3233/jad-180755

Bautch, V. L. (2011). Stem cells and the vasculature. *Nature Medicine, 17*(11), 1437-1443. doi:10.1038/nm.2539

Chong, D. C., Yu, Z. X., Brighton, H. E., Bear, J. E., & Bautch, V. L. (2017). Tortuous Microvessels Contribute to Wound Healing via Sprouting Angiogenesis. *Arteriosclerosis Thrombosis and Vascular Biology, 37*(10), 1903-+. doi:10.1161/atvbaha.117.309993

Claser, C., Nguee, S. Y. T., Balachander, A., Wu Howland, S., Becht, E., Gunasegaran, B., . . . Renia, L. (2019). Lung endothelial cell antigen cross-presentation to CD8. *Nat Commun, 10*(1), 4241. doi:10.1038/s41467-019-12017-8

Cleuren, A. C. A., van der Ent, M. A., Jiang, H., Hunker, K. L., Yee, A., Siemieniak, D. R., . . . Ginsburg, D. (2019). The in vivo endothelial cell translatome is highly heterogeneous across vascular beds. *Proceedings of the National Academy of Sciences of the United States of America, 116*(47), 23618-23624. doi:10.1073/pnas.1912409116

Durinck, S., Spellman, P. T., Birney, E., & Huber, W. (2009). Mapping identifiers for the integration of genomic datasets with the R/Bioconductor package biomaRt. *Nat Protoc, 4*(8), 1184-1191. doi:10.1038/nprot.2009.97

Eberwine, J., Sul, J. Y., Bartfai, T., & Kim, J. (2014). The promise of single-cell sequencing. *Nat Methods, 11*(1), 25-27. doi:10.1038/nmeth.2769

Fischer, D. S., Theis, F. J., & Yosef, N. (2018). Impulse model-based differential expression analysis of time course sequencing data. *Nucleic Acids Res, 46*(20), e119. doi:10.1093/nar/gky675

Gu, C. (2013). *Smoothing Spline ANOVA Models*: Springer New York.

Gunawardana, H., Romero, T., Yao, N., Heidt, S., Mulder, A., Elashoff, D. A., & Valenzuela, N. M. (2021). Tissue-specific endothelial cell heterogeneity contributes to unequal inflammatory responses. *Sci Rep, 11*(1), 1949. doi:10.1038/s41598-020-80102-w

Haimon, Z., Volaski, A., Orthgiess, J., Boura-Halfon, S., Varol, D., Shemer, A., . . . Jung, S. (2018). Re-evaluating microglia expression profiles using RiboTag and cell isolation strategies. *Nat Immunol, 19*(6), 636-644. doi:10.1038/s41590-018-0110-6

Jafarzadeh, S. R., Thomas, B. S., Warren, D. K., Gill, J., & Fraser, V. J. (2016). Longitudinal Study of the Effects of Bacteremia and Sepsis on 5-year Risk of Cardiovascular Events. *Clinical Infectious Diseases, 63*(4), 495-500. doi:10.1093/cid/ciw320

Jambusaria, A., Hong, Z., Zhang, L., Srivastava, S., Jana, A., Toth, P. T., . . . Rehman, J. (2020). Endothelial heterogeneity across distinct vascular beds during homeostasis and inflammation. *Elife, 9*. doi:10.7554/eLife.51413

Kakihana, Y., Ito, T., Nakahara, M., Yamaguchi, K., & Yasuda, T. (2016). Sepsis-induced myocardial dysfunction: pathophysiology and management. *Journal of Intensive Care, 4*, 10. doi:10.1186/s40560-016-0148-1

Kalogeris, T., Baines, C. P., Krenz, M., & Korthuis, R. J. (2012). CELL BIOLOGY OF ISCHEMIA/REPERFUSION INJURY. In K. W. Jeon (Ed.), *International Review of Cell and Molecular Biology, Vol 298* (Vol. 298, pp. 229-317). San Diego: Elsevier Academic Press Inc.

Kalucka, J., de Rooij, L. P. M. H., Goveia, J., Rohlenova, K., Dumas, S. J., Meta, E., . . . Carmeliet, P. (2020). Single-Cell Transcriptome Atlas of Murine Endothelial Cells. *Cell, 180*(4), 764-779.e720. doi:10.1016/j.cell.2020.01.015

Kuleshov, M. V., Jones, M. R., Rouillard, A. D., Fernandez, N. F., Duan, Q., Wang, Z., . . . Ma'ayan, A. (2016). Enrichr: a comprehensive gene set enrichment analysis web server 2016 update. *Nucleic Acids Res, 44*(W1), W90-97. doi:10.1093/nar/gkw377

Laksitorini, M. D., Yathindranath, V., Xiong, W., Hombach-Klonisch, S., & Miller, D. W. (2019). Modulation of Wnt/beta-catenin signaling promotes blood-brain barrier phenotype in cultured brain endothelial cells. *Scientific Reports, 9*, 13. doi:10.1038/s41598-019-56075-w

Liao, J. K. (2013). Linking endothelial dysfunction with endothelial cell activation. *J Clin Invest, 123*(2), 540-541. doi:10.1172/JCI66843

Liu, L. M., Wan, W. B., Xia, S. J., Kalionis, B., & Li, Y. M. (2014). Dysfunctional Wnt/beta-catenin signaling contributes to blood-brain barrier breakdown in Alzheimer's disease. *Neurochemistry International, 75*, 19-25. doi:10.1016/j.neuint.2014.05.004

Liu, M. L., Zhang, L. H., Marsboom, G., Jambusaria, A., Xiong, S. Q., Toth, P. T., . . . Malik, A. B. (2019). Sox17 is required for endothelial regeneration following inflammation-induced vascular injury. *Nature Communications, 10*, 14. doi:10.1038/s41467-019-10134-y

Love, M. I., Huber, W., & Anders, S. (2014). Moderated estimation of fold change and dispersion for RNA-seq data with DESeq2. *Genome Biol, 15*(12), 550. doi:10.1186/s13059-014-0550-8

Lukowski, S. W., Patel, J., Andersen, S. B., Sim, S. L., Wong, H. Y., Tay, J., . . . Khosrotehrani, K. (2019). Single-Cell Transcriptional Profiling of Aortic Endothelium Identifies a Hierarchy from Endovascular Progenitors to Differentiated Cells. *Cell Rep, 27*(9), 2748-2758.e2743. doi:10.1016/j.celrep.2019.04.102

Manukjan, N., Ahmed, Z., Fulton, D., Blankesteijn, W. M., & Foulquier, S. (2020). A Systematic Review of WNT Signaling in Endothelial Cell Oligodendrocyte Interactions: Potential Relevance to Cerebral Small Vessel Disease. *Cells, 9*(6). doi:10.3390/cells9061545

Martowicz, A., Trusohamn, M., Jensen, N., Wisniewska-Kruk, J., Corada, M., Ning, F. C., . . . Nyqvist, D. (2019). Endothelial beta-Catenin Signaling Supports Postnatal Brain and Retinal Angiogenesis by Promoting Sprouting, Tip Cell Formation, and VEGFR (Vascular Endothelial Growth Factor Receptor) 2 Expression. *Arteriosclerosis Thrombosis and Vascular Biology, 39*(11), 2273-2288. doi:10.1161/atvbaha.119.312749

McCarthy, D. J., Chen, Y., & Smyth, G. K. (2012). Differential expression analysis of multifactor RNA-Seq experiments with respect to biological variation. *Nucleic Acids Res, 40*(10), 4288-4297. doi:10.1093/nar/gks042

Metwally, A. A., Yang, J., Ascoli, C., Dai, Y., Finn, P. W., & Perkins, D. L. (2018). MetaLonDA: a flexible R package for identifying time intervals of differentially abundant features in metagenomic longitudinal studies. *Microbiome, 6*(1), 32. doi:10.1186/s40168-018-0402-y

Nolan, D. J., Ginsberg, M., Israely, E., Palikuqi, B., Poulos, M. G., James, D., . . . Rafii, S. (2013). Molecular signatures of tissue-specific microvascular endothelial cell heterogeneity in organ maintenance and regeneration. *Dev Cell, 26*(2), 204-219. doi:10.1016/j.devcel.2013.06.017

Nueda, M. J., Tarazona, S., & Conesa, A. (2014). Next maSigPro: updating maSigPro bioconductor package for RNA-seq time series. *Bioinformatics, 30*(18), 2598-2602. doi:10.1093/bioinformatics/btu333

Paik, D. T., Tian, L., Williams, I. M., Rhee, S., Zhang, H., Liu, C., . . . Wu, J. C. (2020). Single-Cell RNA Sequencing Unveils Unique Transcriptomic Signatures of Organ-Specific Endothelial Cells. *Circulation, 142*(19), 1848-1862. doi:10.1161/CIRCULATIONAHA.119.041433

Pober, J. S., & Sessa, W. C. (2007). Evolving functions of endothelial cells in inflammation. *Nat Rev Immunol, 7*(10), 803-815. doi:10.1038/nri2171

Potente, M., & Mäkinen, T. (2017). Vascular heterogeneity and specialization in development and disease. *Nat Rev Mol Cell Biol, 18*(8), 477-494. doi:10.1038/nrm.2017.36

Ritchie, M. E., Phipson, B., Wu, D., Hu, Y., Law, C. W., Shi, W., & Smyth, G. K. (2015). limma powers differential expression analyses for RNA-sequencing and microarray studies. *Nucleic Acids Res, 43*(7), e47. doi:10.1093/nar/gkv007

Roivainen, M., Viik-Kajander, M., Palosuo, T., Toivanen, P., Leinonen, M., Saikku, P., . . . Manttari, M. (2000). Infections, inflammation, and the risk of coronary heart disease. *Circulation, 101*(3), 252-257. doi:10.1161/01.cir.101.3.252

Sabbagh, M. F., Heng, J. S., Luo, C., Castanon, R. G., Nery, J. R., Rattner, A., . . . Nathans, J. (2018). Transcriptional and epigenomic landscapes of CNS and non-CNS vascular endothelial cells. *Elife, 7*. doi:10.7554/eLife.36187

Sanz, E., Yang, L., Su, T., Morris, D. R., McKnight, G. S., & Amieux, P. S. (2009). Cell-type-specific isolation of ribosome-associated mRNA from complex tissues. *Proc Natl Acad Sci U S A, 106*(33), 13939-13944. doi:10.1073/pnas.0907143106

Senaldi, G., Vesin, C., Chang, R., Grau, G. E., & Piguet, P. F. (1994). Role of polymorphonuclear neutrophil leukocytes and their integrin CD11a (LFA-1) in the pathogenesis of severe murine malaria. *Infect Immun, 62*(4), 1144-1149. doi:10.1128/IAI.62.4.1144-1149.1994

Su, T., Stanley, G., Sinha, R., D'Amato, G., Das, S., Rhee, S., . . . Red-Horse, K. (2018). Single-cell analysis of early progenitor cells that build coronary arteries. *Nature, 559*(7714), 356-362. doi:10.1038/s41586-018-0288-7

Tiruppathi, C., Minshall, R. D., Paria, B. C., Vogel, S. M., & Malik, A. B. (2002). Role of Ca2+ signaling in the regulation of endothelial permeability. *Vascul Pharmacol, 39*(4-5), 173-185. doi:10.1016/s1537-1891(03)00007-7

Tombor, L. S., John, D., Glaser, S. F., Luxán, G., Forte, E., Furtado, M., . . . Dimmeler, S. (2021). Single cell sequencing reveals endothelial plasticity with transient mesenchymal activation after myocardial infarction. *Nature Communications, 12*. doi:https://doi.org/10.1038/s41467-021-20905-1

van den Brink, S. C., Sage, F., Vértesy, Á., Spanjaard, B., Peterson-Maduro, J., Baron, C. S., . . . van Oudenaarden, A. (2017). Single-cell sequencing reveals dissociation-induced gene expression in tissue subpopulations. *Nat Methods, 14*(10), 935-936. doi:10.1038/nmeth.4437

Vanlandewijck, M., He, L., Mäe, M. A., Andrae, J., Ando, K., Del Gaudio, F., . . . Betsholtz, C. (2018). A molecular atlas of cell types and zonation in the brain vasculature. *Nature, 554*(7693), 475-480. doi:10.1038/nature25739

Yu, G., Wang, L. G., Han, Y., & He, Q. Y. (2012). clusterProfiler: an R package for comparing biological themes among gene clusters. *OMICS, 16*(5), 284-287. doi:10.1089/omi.2011.0118

Yucel, G., Zhao, Z. H., El-Battrawy, I., Lan, H., Lang, S., Li, X., . . . Akin, I. (2017). Lipopolysaccharides induced inflammatory responses and electrophysiological dysfunctions in human-induced pluripotent stem cell derived cardiomyocytes. *Scientific Reports, 7*, 13. doi:10.1038/s41598-017-03147-4

Yucel, N., Axsom, J., Yang, Y., Li, L., Rhoades, J. H., & Arany, Z. (2020). Cardiac endothelial cells maintain open chromatin and expression of cardiomyocyte myofibrillar genes. *Elife, 9*. doi:10.7554/eLife.55730

Figures

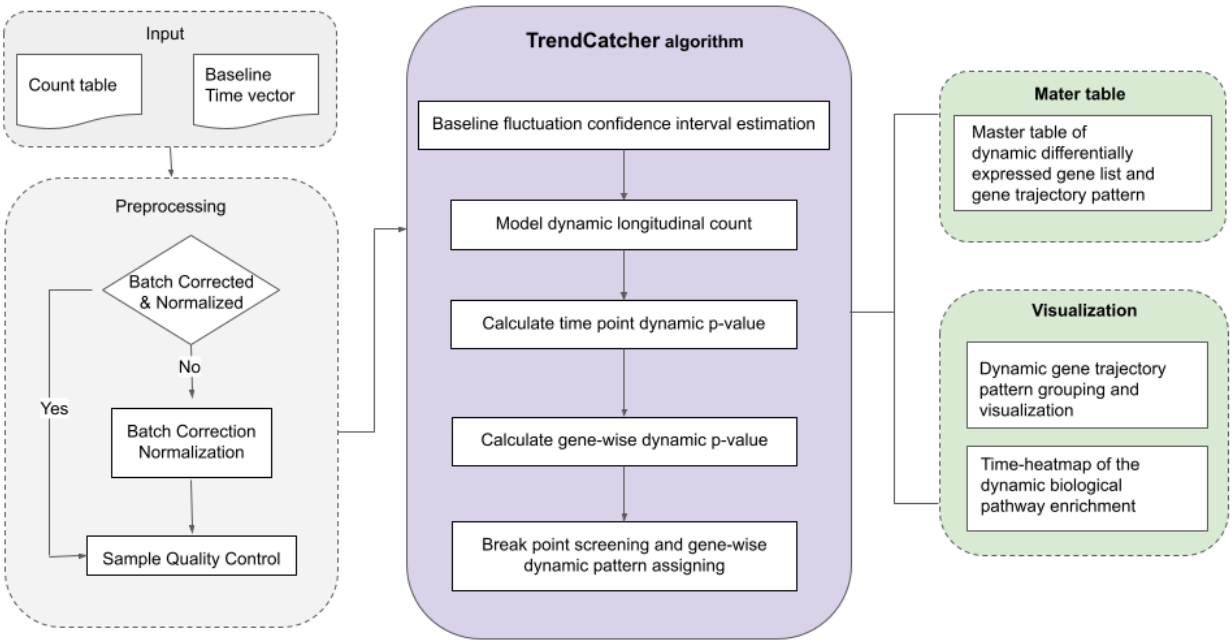

Figure 1. TrendCatcher Framework

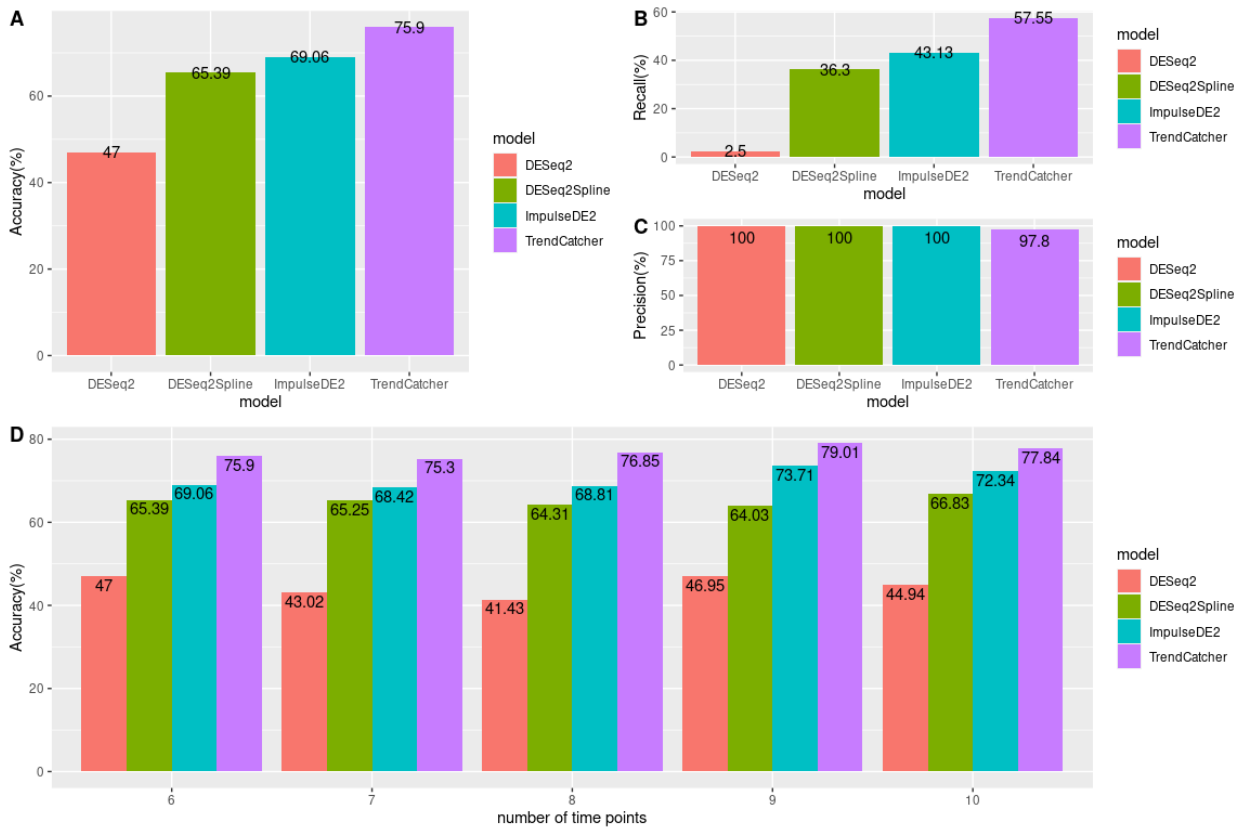

Figure 2. TrendCatcher prediction performance. (**A**) Prediction accuracy compared to DESeq2, DESeq2Spline and ImpulseDE2 model with mixed types of trajectory patterns. (**B**) Prediction recall from the same simulated dataset with (**A**). (**C**) Prediction precision from the same simulated dataset with (**A**). **(D)** Prediction accuracy compared to DESeq2, DESeq2Spline and ImpulseDE2 model with various number of time points, from 6 to 10, using mixed types of trajectory patterns.

A

	Brain ECs	Heart ECs	Lung ECs
Up_down	1,456	1,712	1,601
Down_up	506	210	660
up	35	94	183
Down_up_down	30	2	16
Up_down_up_down	9	15	92
Up_down_up	8	8	38
Down	2	2	13
Down_up_down_up	1	1	29
Total	2,047	2,044	2,632

B

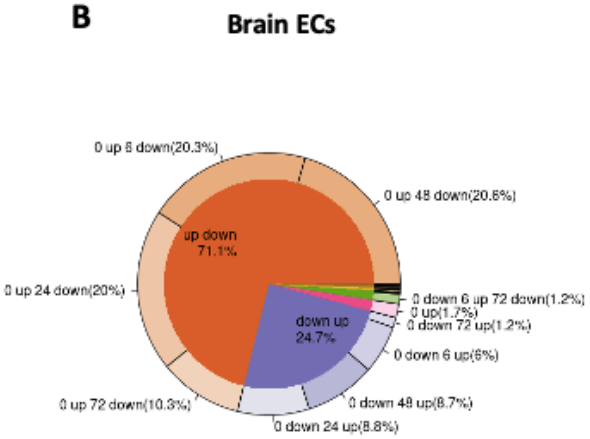

C

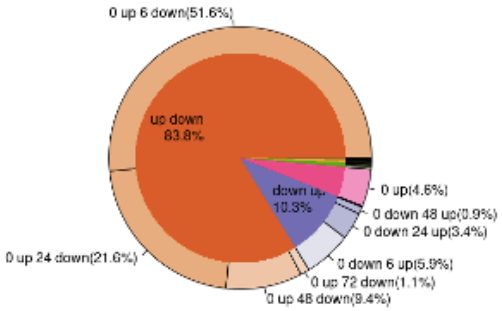

D

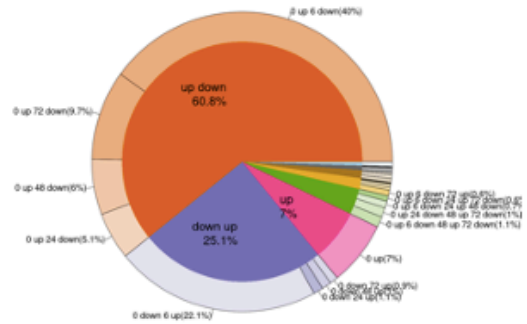

Figure 3. Dynamic gene composition comparison among brain, heart and lung ECs. **(A)** Number of different types of dynamic gene trajectories belonged to each master-pattern. **(B)** Hierarchical pie chart of brain EC, inner pie is master-pattern composition, outer pie is sub-pattern composition. **(C)** Hierarchical pie chart of heart EC. **(D)** Hierarchical pie chart of lung EC.

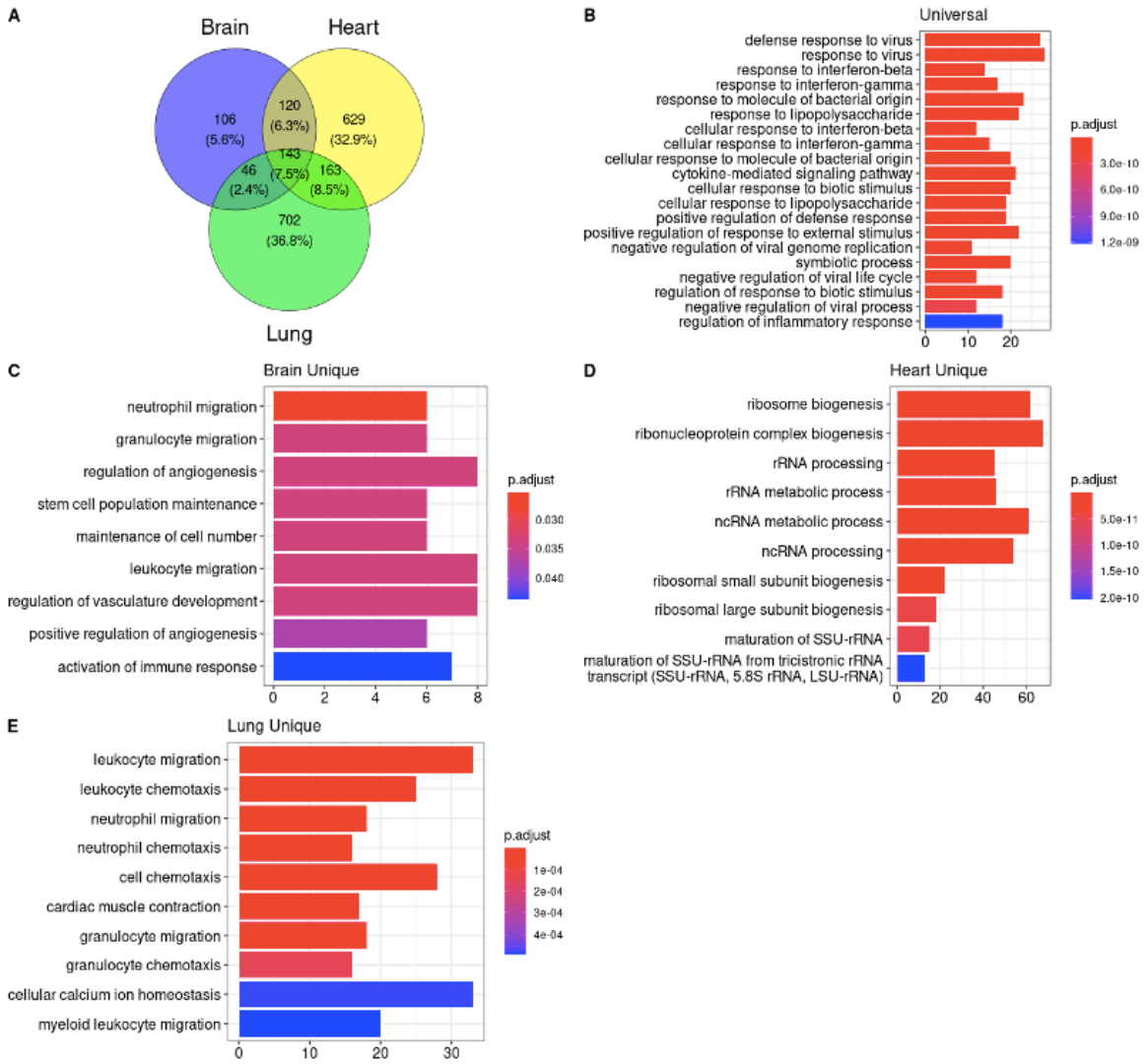

Figure 4. Organ-universal inflammatory response, and organ-specific inflammatory response for trajectory sub-pattern, "0h_up_6h_down_168h". **(A)** Venn diagram of dynamic genes from sub-pattern "0h_up_6h_down_18h" across brain, heart and lung ECs. **(B)** GO enrichment for the overlapped 143 dynamic genes. X-axis is the number of genes, y-axis is GO term, p-value is the enrichment p-value for each GO term. **(C)** GO enrichment analysis for 106 genes only found in brain EC. **(D)** GO enrichment analysis for 629 genes only found in heart EC. **(E)** GO enrichment analysis for 702 genes only found in lung EC.

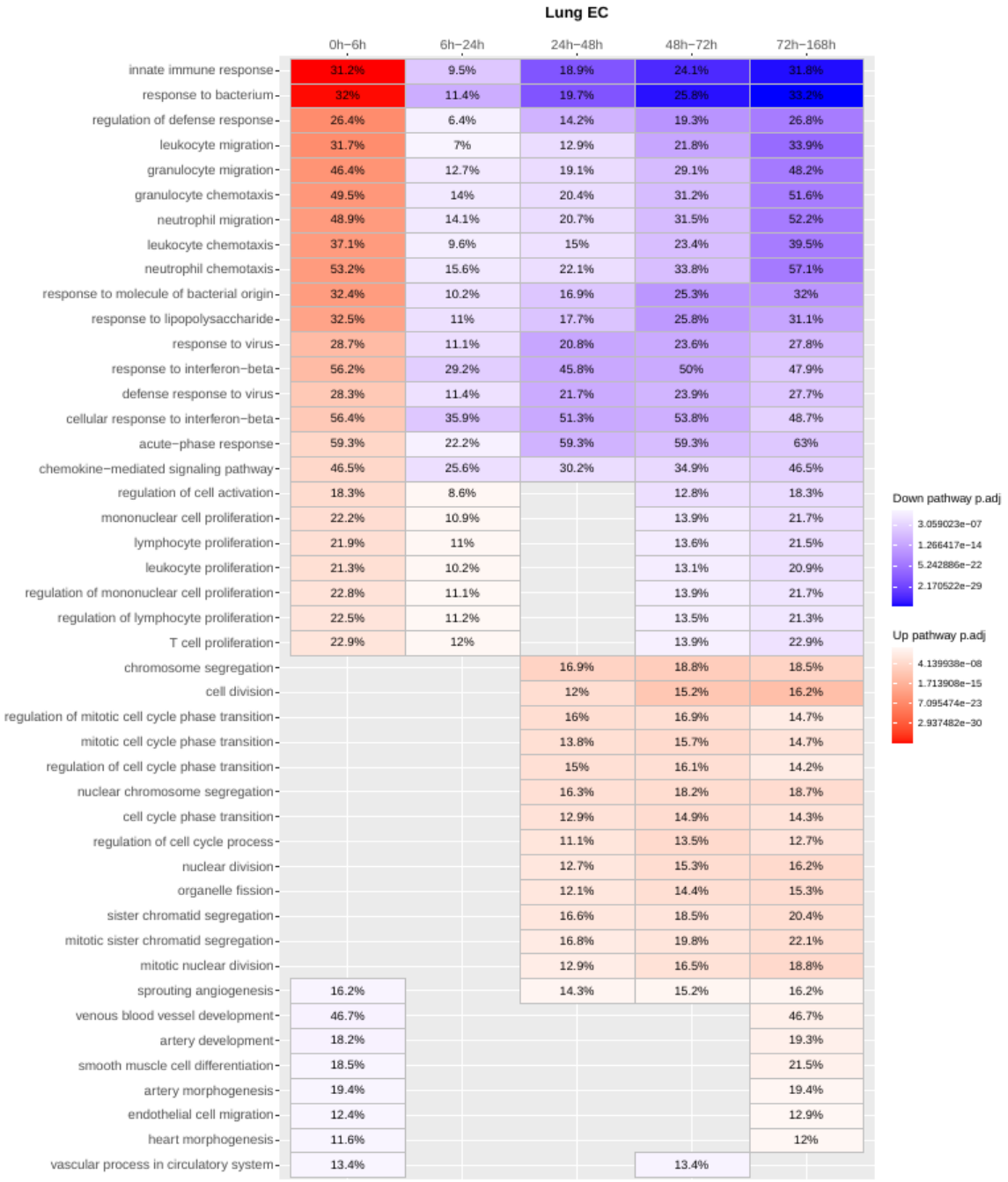

Figure 5. Time-heatmap of lung ECs. Each column represents a time window, each row represents a significantly enriched (p-value <0.05) GO term. Red shade represents GO term are upregulated compared to the previous break point. Blue shade represents GO term are down regulated compared to the previous break point. Percentage number within each tile represents the percentage of genes belongs to the corresponding GO term are dynamic and captured by TrendCatcher. Shade of the color represents the enrichment p-value, the darker the shade is, the more significantly enriched from GO enrichment analysis.

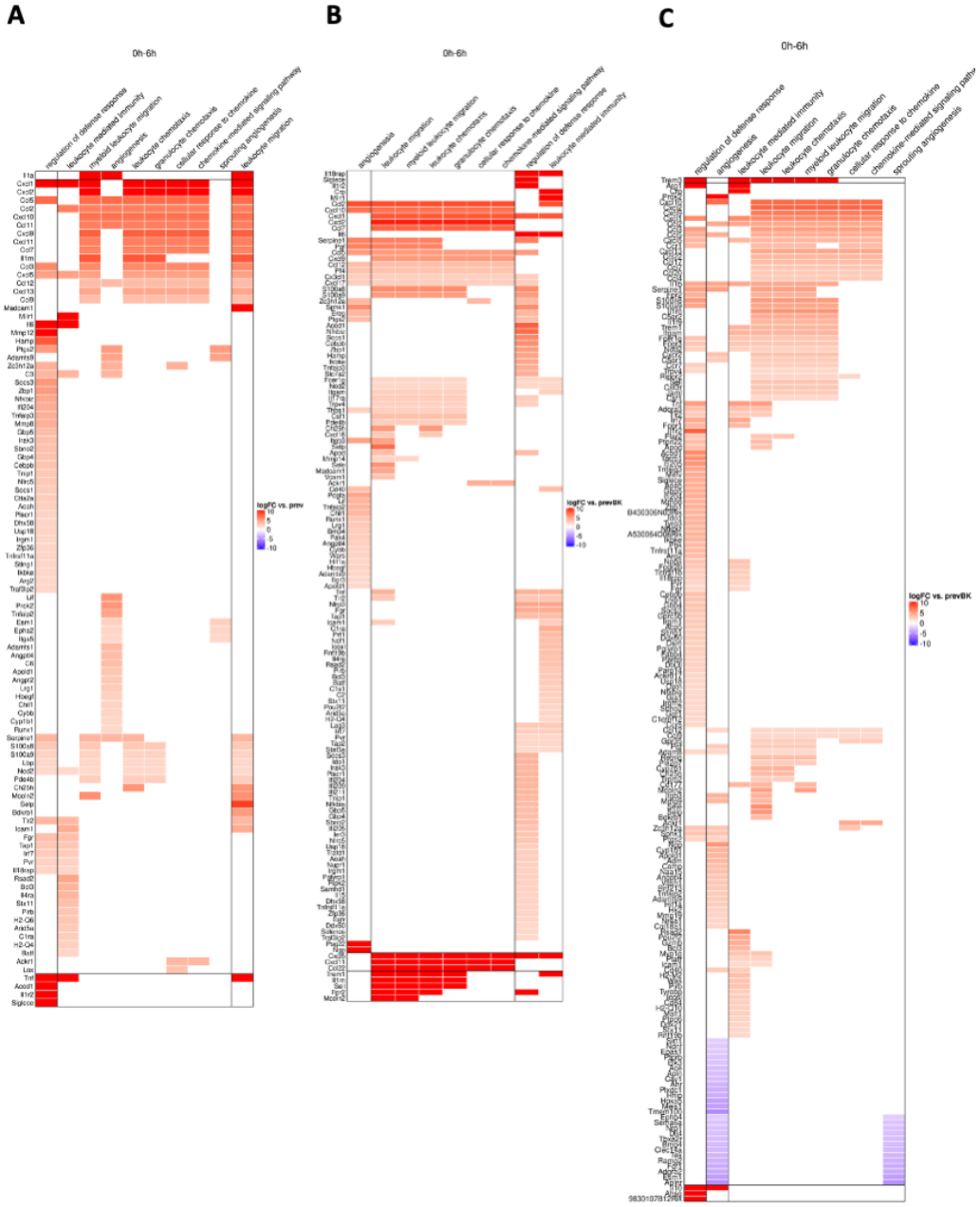

Figure 6. GO-Heatmap. For time window 0h-6h, from selected pathways, including "regulation of defense response", "leukocyte migration", "myeloid leukocyte migration", "leukocyte chemotaxis", "granulocyte chemotaxis", "cellular response to chemokine", "chemokine-mediated signaling pathway", "angiogenesis", "sprouting angiogenesis", "response to bacterium", "leukocyte mediated immunity". Dynamic genes from each organ. **(A)** Brain EC. **(B)** Heart EC. **(C)** Lung EC. The color shade represent log fold change magnitude. Red means up-regulated, blue means down-regulated.

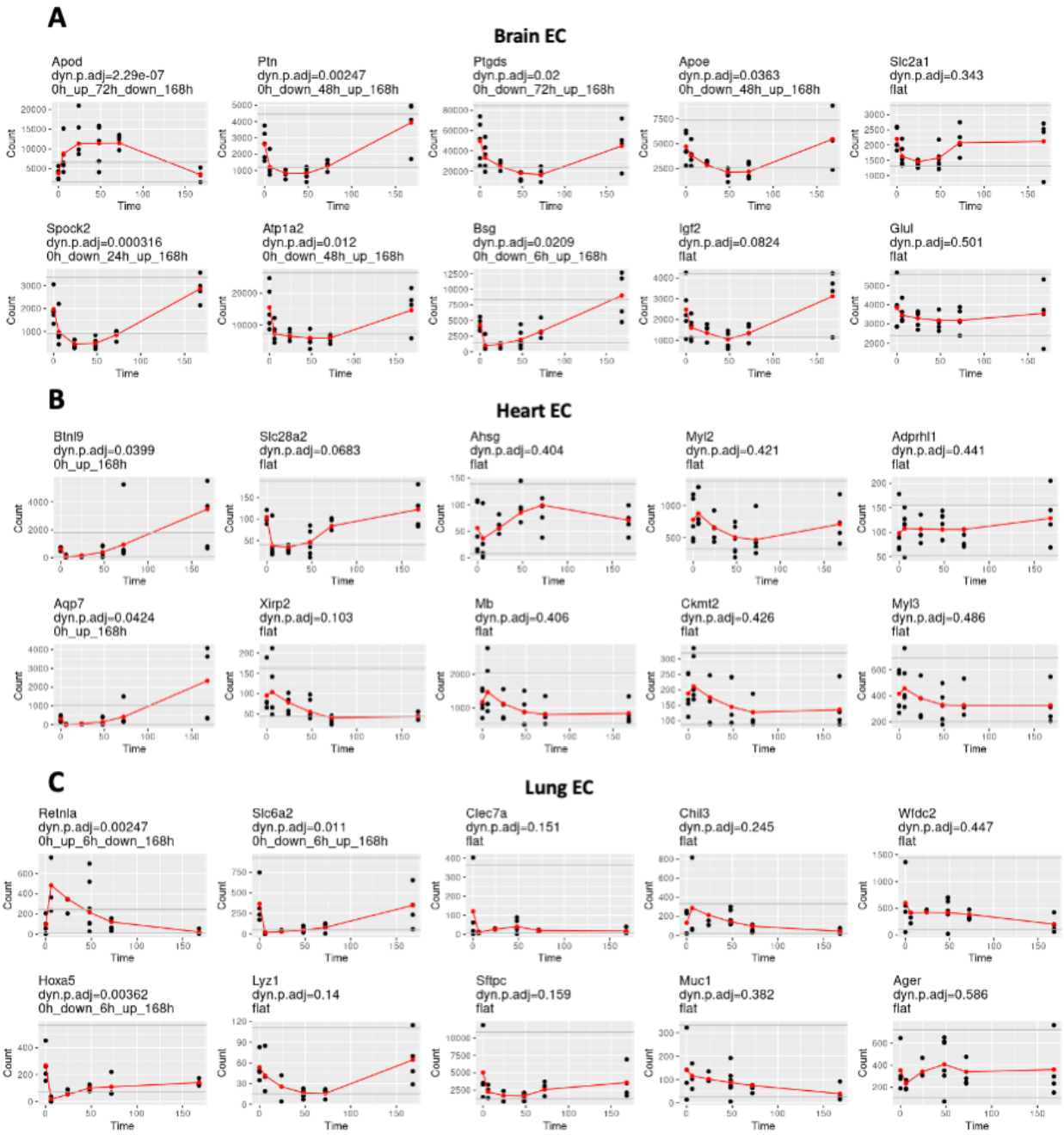

Figure 7. Top 10 organ-specific RiboTag EC signature genes dynamic trajectories. (**A**) Brain ECs top 10 signature genes trajectories, with gene symbol, dynamic p-value from TrendCatcher and its trajectory pattern. (**B**) Heart ECs top 10 signature genes trajectories. (**C**) Lung ECs top 10 signature genes trajectories. *dyn.p.adj* is the adjusted dynamic p-value from TrendCatcher. Black dots are observed count data for each time point for each gene. Red line is smoothed ANOVA spline fitting. Grey lines are baseline fluctuation intervals constructed using constant NB model.

Figure Supplement

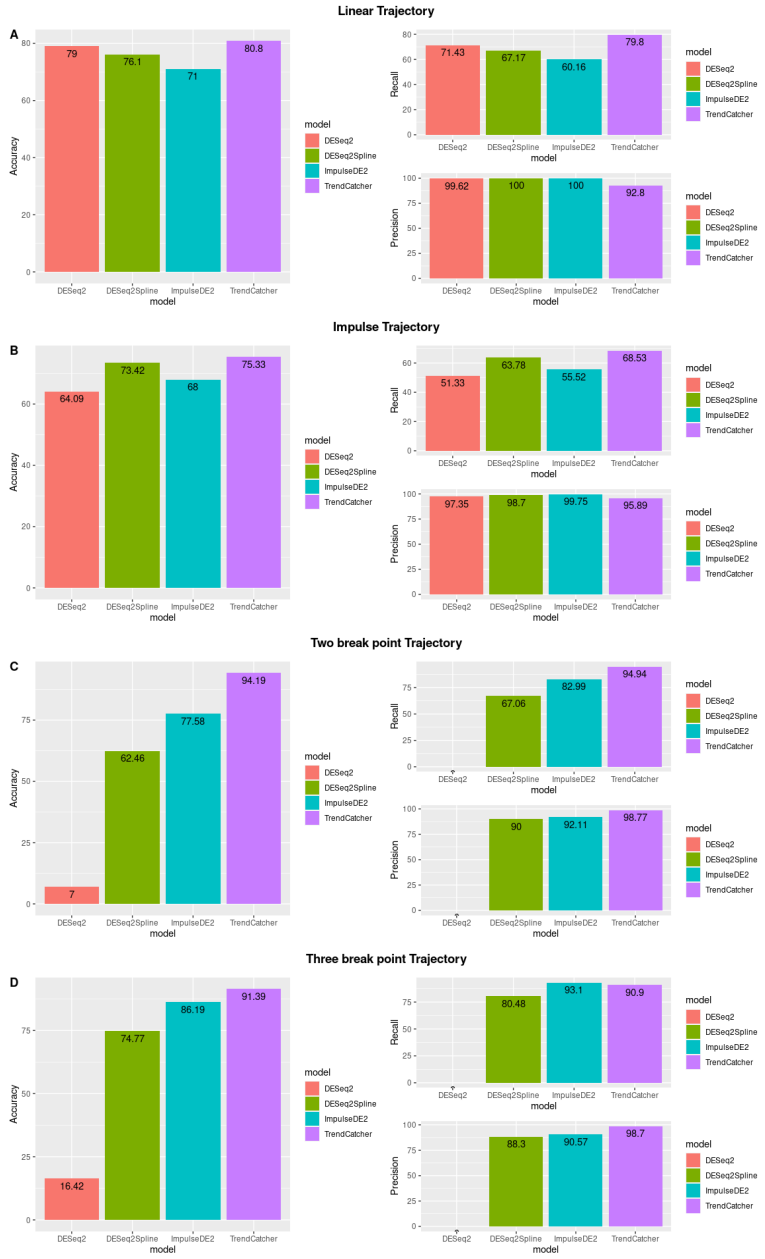

Figure 2-figure supplement 1. TrendCatcher prediction performance across different types of trajectories. (**A**) Prediction accuracy (left), recall (top-right) and precision (bottom-right), compared to DESeq2, DESeq2Spline and ImpulseDE2 model with linear trajectories. (**B**) Prediction accuracy (left), recall (top-right) and precision (bottom-right), compared to DESeq2, DESeq2Spline and ImpulseDE2 model with impulse trajectories. (**C**) Prediction accuracy (left), recall (top-right) and precision (bottom-right), compared to DESeq2, DESeq2Spline and ImpulseDE2 model with two break points trajectories. (**D**) Prediction accuracy (left), recall (top-right) and precision (bottom-right), compared to DESeq2, DESeq2Spline and ImpulseDE2 model with three break points trajectories.

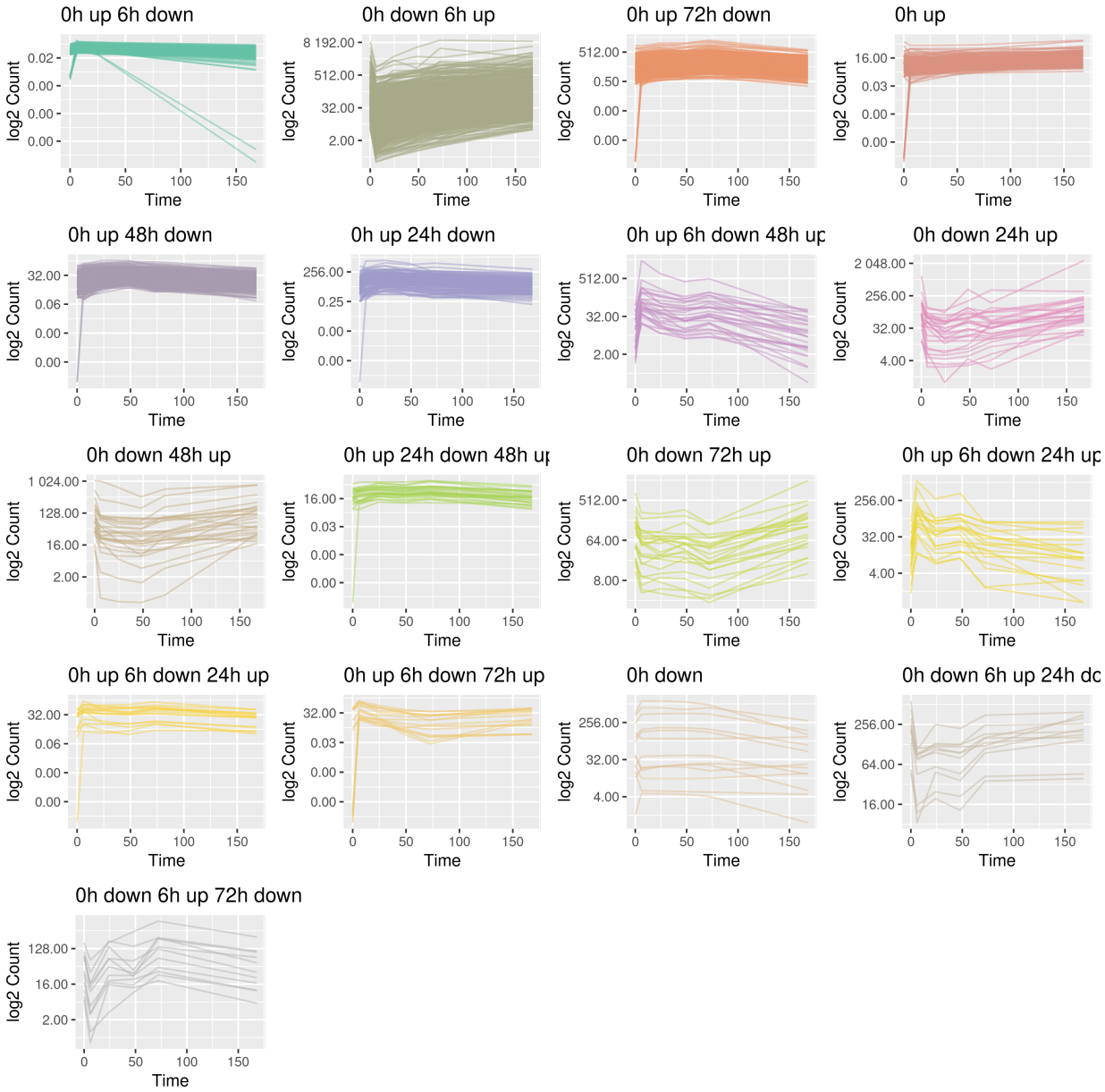

698
699 **Figure 3–figure supplement 1.** Top sub-pattern dynamic gene trajectories in lung ECs. Ranked
700 by the number of sub-pattern trajectory type. "0h up 48h down" means gene upregulated in the
701 first 48 hours and then downregulated from 48 hours to 168 hours. X-axis is time (hour), y-axis is
702 the log2 count of RNA-seq reads.
703

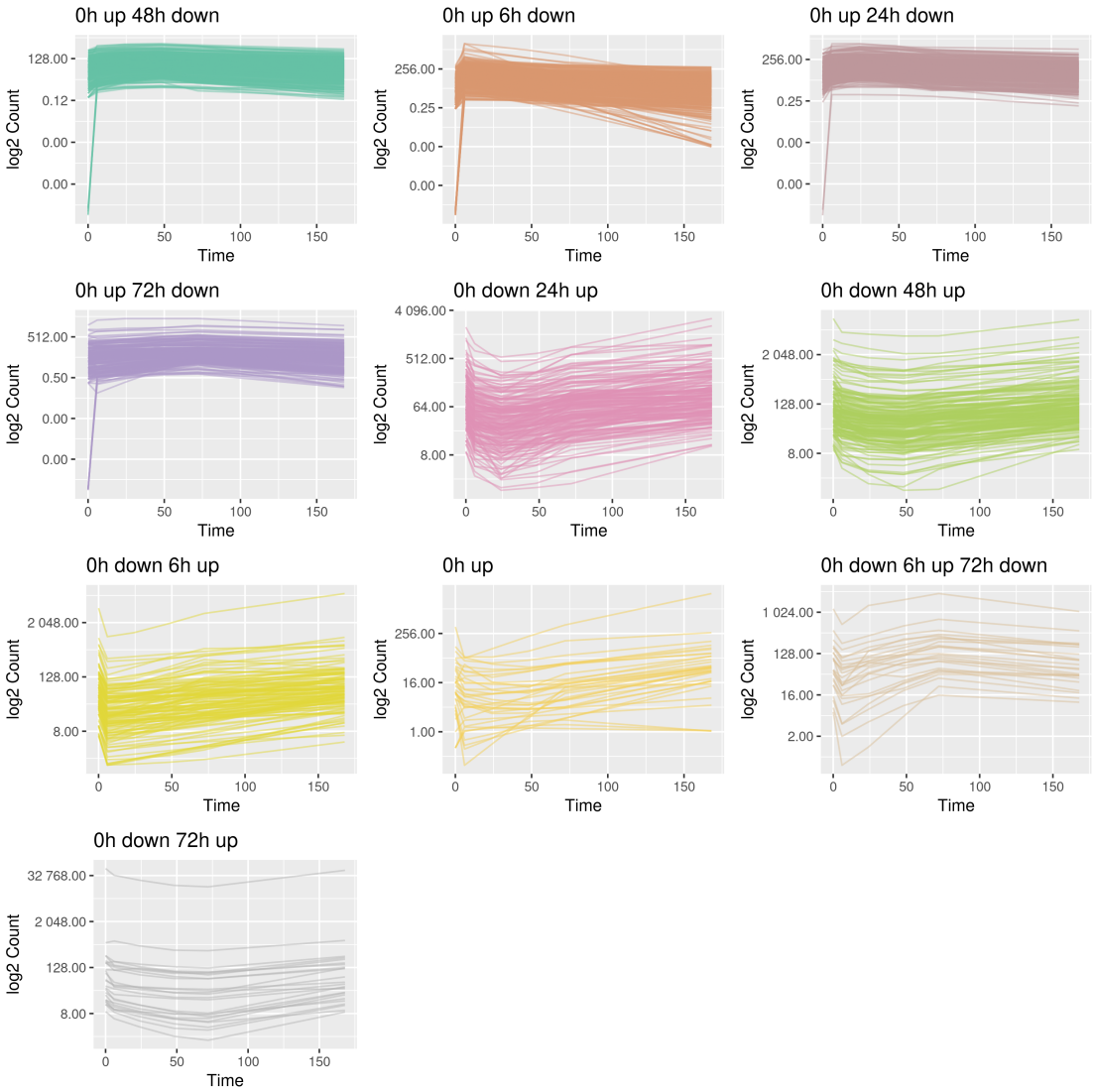

Figure 3–figure supplement 2. Top sub-pattern dynamic gene trajectories in brain ECs. Ranked by the number of sub-pattern trajectory type. X-axis is time (hour), y-axis is the log2 count of RNA-seq reads

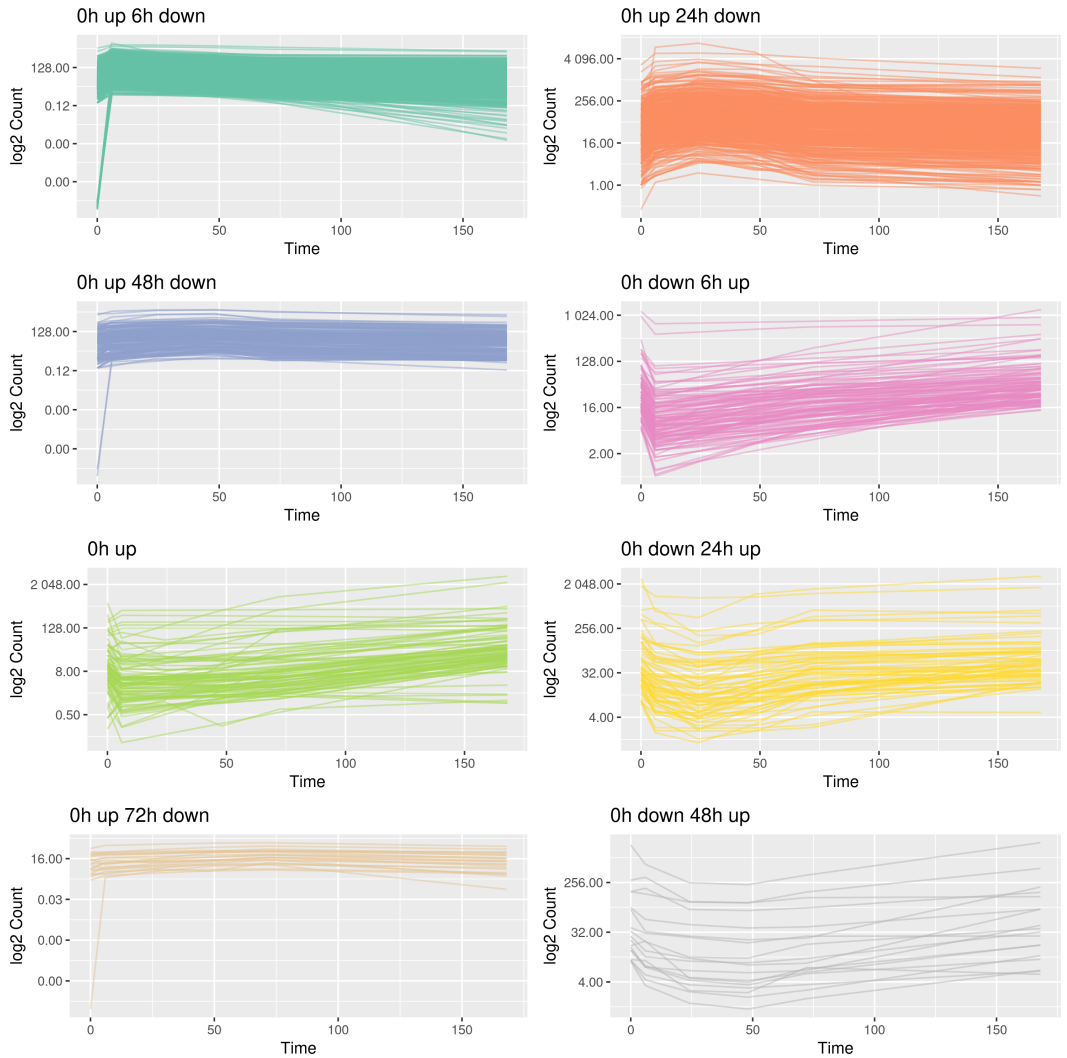

Figure 3–figure supplement 3. Top sub-pattern dynamic gene trajectories in heart ECs. Ranked by the number of sub-pattern trajectory type. X-axis is time (hour), y-axis is the log2 count of RNA-seq reads.

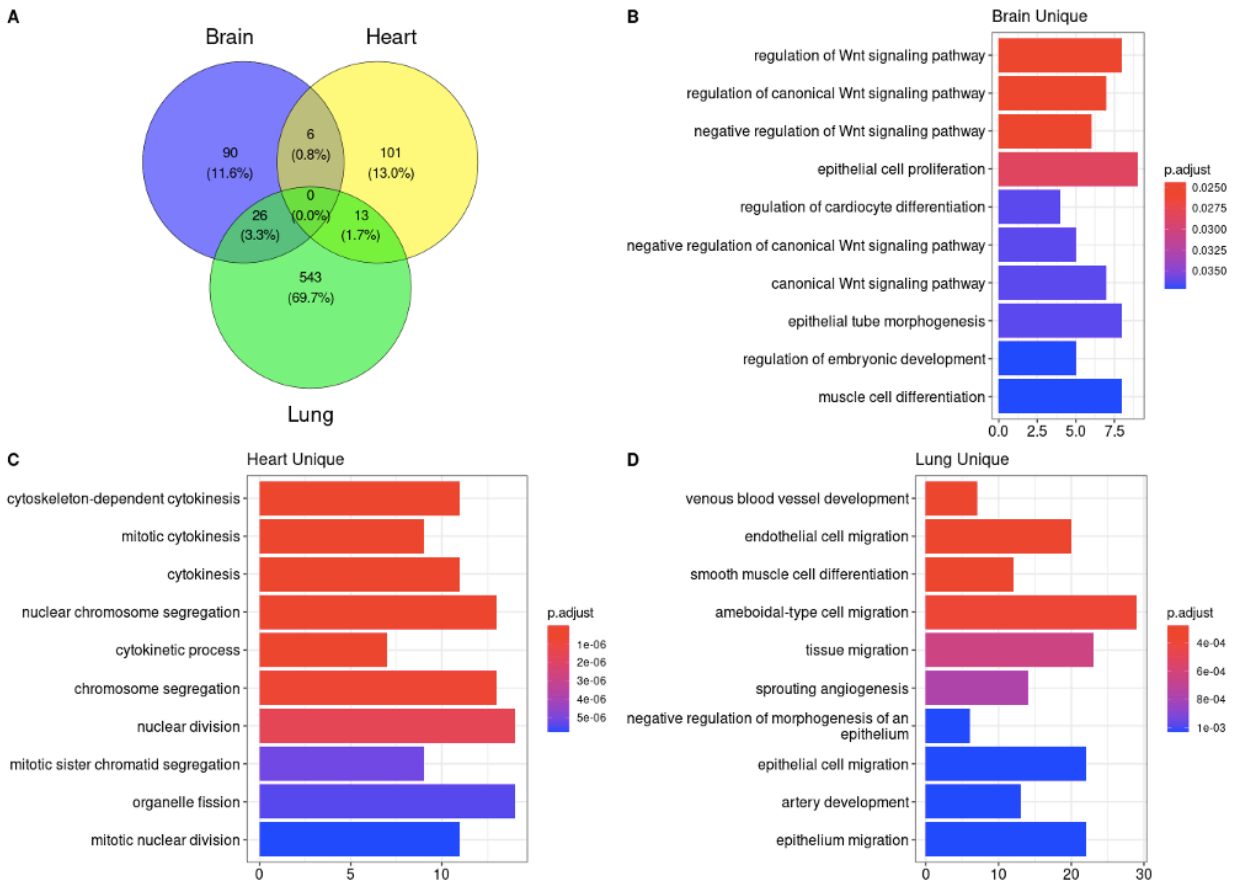

Figure 4–figure supplement 1. Organ-universal inflammatory response, and organ-specific inflammatory response for trajectory sub-pattern, "0h_down_6h_up_168h". (**A**) Venn diagram of dynamic genes from sub-pattern "0h_down_6h_up_168h" across brain, heart and lung ECs. (**B**) GO enrichment analysis for 90 genes only found in brain EC. (**C**) GO enrichment analysis for 101 genes only found in heart EC. (**D**) GO enrichment analysis for 543 genes only found in lung EC.

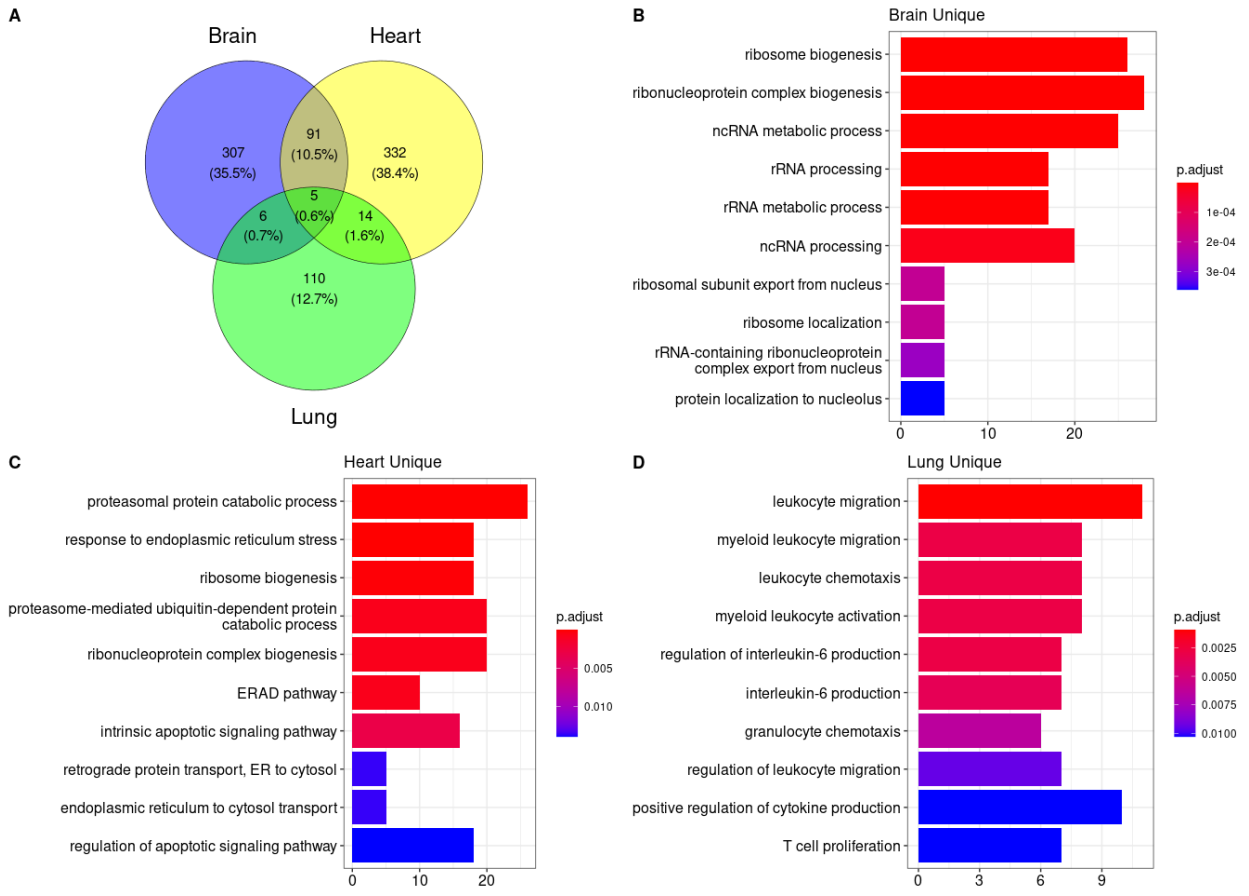

Figure 4–figure supplement 2. Organ-universal inflammatory response, and organ-specific inflammatory response for trajectory sub-pattern, "0h_up_24h_down_168h". (**A**) Venn diagram of dynamic genes from sub-pattern "0h_up_24h_down_168h" across brain, heart and lung ECs. (**B**) GO enrichment analysis for 307 genes only found in brain EC. (**C**) GO enrichment analysis for 332 genes only found in heart EC. (**D**) GO enrichment analysis for 110 genes only found in lung EC.

Figure 5–figure supplement 1. Time-heatmap of brain ECs. Each column represents a time window, each row represents a significantly enriched (p-value <0.05) GO term. Red shade represents GO term are upregulated compared to the previous break point. Blue shade represents GO term are down regulated compared to the previous break point. Percentage number within each tile represents the percentage of genes belongs to the corresponding GO term are dynamic and captured by TrendCatcher. Shade of the color represents the enrichment p-value, the darker the shade is, the more significantly enriched from GO enrichment analysis.

Figure 5–figure supplement 2. Time-heatmap of heart ECs. Each column represents a time window, each row represents a significantly enriched (p-value <0.05) GO term. Red shade represents GO term are upregulated compared to the previous break point. Blue shade represents GO term are down regulated compared to the previous break point. Percentage number within each tile represents the percentage of genes belongs to the corresponding GO term are dynamic and captured by TrendCatcher. Shade of the color represents the enrichment p-value, the darker the shade is, the more significantly enriched from GO enrichment analysis.